Contents lists available at ScienceDirect

Nuclear Inst. and Methods in Physics Research, A

journal homepage: www.elsevier.com/locate/nima



Full Length Article

A simple dynamic time-over-threshold circuit for high-resolution amplitude measurement



Michael Reese

GSI Helmholtzzentrum für Schwerionenforschung GmbH, Planckstraße 1, Darmstadt, 64291, Germany

ARTICLE INFO

Keywords: Dynamic time-over-threshold LaBr3:Ce scintillator readout

ABSTRACT

The dynamic time-over-threshold (dToT) method is a timing-based readout technique for pulse-height measurement of radiation detectors. After the leading-edge detection, the discriminator threshold is raised to allow precise pulse-height estimation over a wide dynamic range. A particularly simple circuit implementation of dToT is presented that delivers excellent amplitude resolution with minimal complexity. Experiments show that the resolution is sufficient to read out high-performance scintillators such as LaBr₃:Ce without degrading their intrinsic energy resolution.

1. Introduction

Conventional scintillation-detector readout techniques, such as charge integration or full waveform digitization, provide excellent energy resolution but typically require complex and costly electronics. The time-over-threshold (ToT) method offers a simple, inexpensive alternative by relating pulse amplitude to the duration that the signal remains above a fixed threshold. However, a static threshold imposes an inherent trade-off between dynamic range and amplitude resolution, limiting the usefulness of the method for high-performance spectroscopy.

The dynamic time-over-threshold (dToT) technique was introduced in [1] and later simplified in [2], demonstrating an energy resolution of 5.18% at 511~keV for a LaBr $_3$:Ce crystal. Nevertheless, this reported resolution still falls short of the intrinsic capability of such high-quality scintillators. The TwinPeaks frontend [3] is another implementation of the time-over-threshold method. It attains excellent timing and energy resolution by splitting the signal into two branches optimized separately for timing and amplitude measurements. However it adds complexity and occupies two TDC channels in order to measure a single signal.

In this work, a very simple implementation of the dToT principle is presented. Its performance was experimentally verified with a cylindrical 1×1 inch LaBr $_3$:Ce detector. The design retains the RC-feedback network of Ref. [1] but connects it directly to the comparator output, eliminating the monostable timing circuit. In addition, the input CRRC filter is removed, and the circuit is placed directly at the detector so that pulse shaping is provided only by the detector capacitance and the input impedance of the dToT stage. Measurements show that this minimalist design achieves amplitude resolution sufficient to preserve the

intrinsic energy resolution of LaBr₃:Ce, demonstrating that dToT can provide a practical, low-cost solution for high-resolution spectroscopy. The leading-edge timing properties are largely preserved, though they do not fully match the intrinsic timing performance of the scintillator.

2. The circuit

The simplified circuit is shown in Fig. 1. It was connected directly to the photomultipler anode of the detector. The high input impedance allows the detector capacitance to perform charge integration without degrading the slope of the rising edge, preserving the timing information in the leading edge of the pulse. A low-noise, high-input-impedance NSVJ6904 J-FET pair is used as a differential amplifier, providing moderate voltage gain¹ while maintaining excellent noise performance. The constant-current source in the differential amplifier is implemented with a current mirror using a BFS481 dual NPN transistor.

The LT1720 comparator inputs are connected directly to the outputs of the differential amplifier. A voltage divider and low-pass filter provide feedback from the comparator output to the second input of the differential amplifier, establishing a dynamic threshold. With this topology, the threshold is driven towards one of two values: a high level $V_{\rm high}$ when the signal is above threshold, and a low level $V_{\rm low}$ when the signal is below threshold. The low-pass filter limits the rate of change of the threshold between $V_{\rm high}$ and $V_{\rm low}$ to the time constant $\tau_{\rm fb} = R_{\rm fb}\,C_{\rm fb}$ of the feedback network. The time constant $\tau_{\rm fb}$ must be equal to or larger than the input time constant $\tau_{\rm inp} = R\,C$, where C is the detector capacitance and R is the circuit input impedance. Otherwise, the dynamic threshold will oscillate around the trailing edge

E-mail address: m.reese@gsi.de.

¹ SPICE simulation indicates a voltage gain of approximately ×10, which was not verified experimentally.

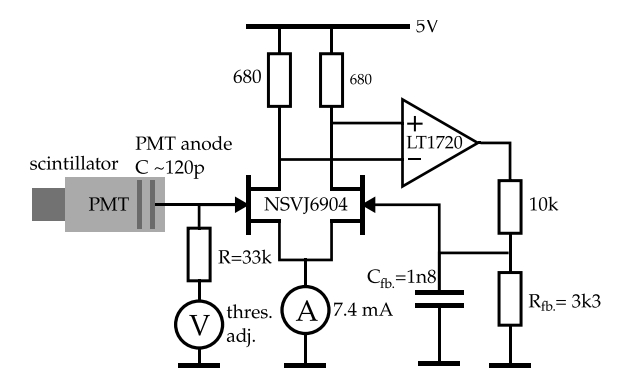


Fig. 1. Simplified schematic of the circuit showing the main components: high-impedance differential amplifier, comparator, and feedback network. Details like the LVDS output driver or input voltage filtering are not shown.

of the signal. If $V_{\rm low}$ is very close to the signal baseline and $\tau_{\rm fb}=\tau_{\rm inp}$, the threshold will closely follow the trailing edge of the signal because the low comparator output draws the threshold back to $V_{\rm low}$, as shown in Fig. 2. In this case, very little distortion is expected in the dToT measurement of a subsequent signal, even if it is detected on the tail of the previous pulse. However, this expected behavior at high counting rates has not yet been experimentally verified.

The 10 k Ω resistor at the comparator output was chosen such that the current drawn by the feedback network remains negligible. As will be shown in Section 3, it is beneficial for the energy resolution to maximize the dynamic change of the threshold $V_{\rm high}$. In the prototype circuit, the value of $R_{\rm fb}$ was increased in several steps until the desired energy resolution was achieved, while $C_{\rm fb}$ was decreased accordingly to keep $\tau_{\rm fb}$ constant.

Being a differential amplifier, only the difference between the signal and the dynamic threshold is relevant. In the prototype implementation, the threshold is adjusted by adding a positive offset voltage to the signal. This offset is generated by a $300\,\Omega$ potentiometer divider between the 5 V supply rail and ground. Alternatively, the threshold voltage could be adjusted by applying a negative offset voltage in the feedback path to the other input of the differential amplifier.

The circuit operates without modification for both positive and negative polarity signals, depending on the threshold setting. For positive pulses, the dynamic range is limited to about +2 V; beyond this value, the gate diode of the J-FET conducts, disturbing the RC discharge. For negative pulses, the amplitude is limited only by the gate–drain voltage rating of the J-FET and should not exceed -20 V. Although the amplifier saturates at higher amplitudes, the dToT measurement remains accurate provided that the threshold crossing occurs within the amplifier's linear range.

The comparator output can be directly used to measure the dToT with a time-to-digital converter (TDC). In the prototype, it was routed through an LVDS driver into a TAMEX4 TDC [3] with a bare LVDS input board, i.e. no further processing was done to the LVDS pulses before entering the TDC.

3. Analytical description of idealized behavior

In the following discussion, all voltages are measured relative to the signal baseline, and $V_{\rm low}$ is assumed to be very close to the baseline, i.e., $V_{\rm low}=0$. It is further assumed that the scintillator light decay time $\tau_{\rm sci}$ is short compared to the input time constant $\tau_{\rm inp}$, which is valid for the very fast LaBr3:Ce scintillator with $\tau_{\rm sci}\approx 23\,{\rm ns}$. Finally, the feedback time constant is assumed to match exactly the input time constant, $\tau_{\rm fb}=\tau_{\rm inp}$. Under these idealized conditions, the signal and dynamic threshold behave as illustrated in Fig. 2.

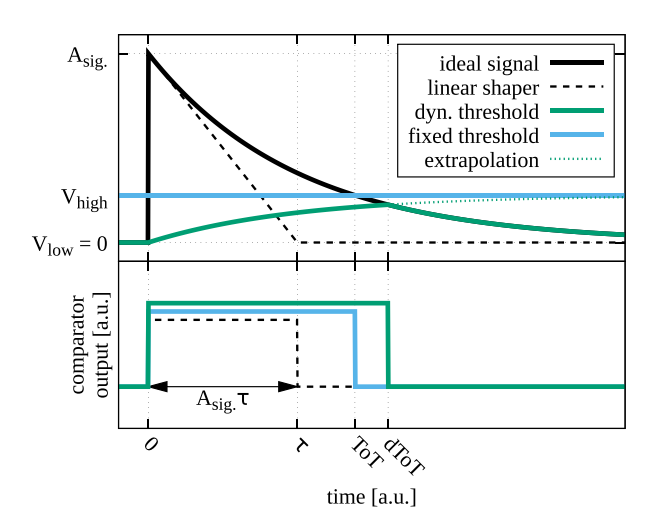


Fig. 2. Top: Idealized signal and dynamic threshold behavior with $V_{\rm low} \to 0$ and $\tau = \tau_{\rm fb} = \tau_{\rm inp}$. The dashed line shows a hypothetical triangular signal with the same time constant for $A_{\rm sig.}=1$. Bottom: the comparator output signal for all three cases.

Analytical expressions for the dToT and its relative uncertainty Δ dToT/dToT can be derived in this scenario. The time-dependent signal shape is given by

$$s(t) = A \exp\left(-\frac{t}{\tau}\right), \quad t > 0,\tag{1}$$

and the dynamic threshold evolves as

$$V(t) = V_{\text{high}} \left(1 - \exp\left(-\frac{t}{\tau}\right) \right), \quad 0 < t < \text{dToT}.$$
 (2)

The dToT is defined by the intersection of s(t) and V(t), yielding

$$dToT(A_{sig}) = \tau \ln \left(\frac{A_{sig}}{V_{high}} + 1 \right).$$
 (3)

The uncertainty in the measured dToT is dominated by the combined noise σ of the signal and threshold, and by the slope of the intersection between the trailing edge of the signal and the dynamically rising threshold:

$$\Delta dToT = \frac{\sigma}{\left|\frac{d}{dt} \left(s(t) - V(t)\right)\right|_{t = dToT}}.$$
(4)

Evaluating the derivative in (4) and dividing by (3) gives the relative uncertainty of the dToT measurement:

$$\frac{\Delta \text{dToT}}{\text{dToT}} = \frac{\sigma}{V_{\text{high}} \ln\left(\frac{A_{\text{sig}}}{V_{\text{high}}} + 1\right)}.$$
 (5)

Notably, this relative uncertainty does not depend on the signal decay time τ , which can therefore be chosen freely by adjusting the input resistor of the circuit. For example, τ can be adapted to the capabilities of the TDC capturing the dToT output. No loss in relative dToT resolution is expected when lengthening the signal for slower TDCs.

For comparison, the relative uncertainty of a non-dynamic ToT measurement of the same pulse shape with a fixed threshold at $V_{\rm high}$ is

$$\frac{\Delta \text{ToT}}{\text{ToT}} = \frac{\sigma}{V_{\text{high}} \ln \left(\frac{A_{\text{sig}}}{V_{\text{high}}}\right)},\tag{6}$$

and for ideal linear pulse shaping with slope $-1/\tau$ and $V_{\rm low} \rightarrow 0$ it is

$$\frac{\Delta \text{lin}}{\text{lin}} = \frac{\sigma}{A_{\text{sig}}}.$$
 (7)

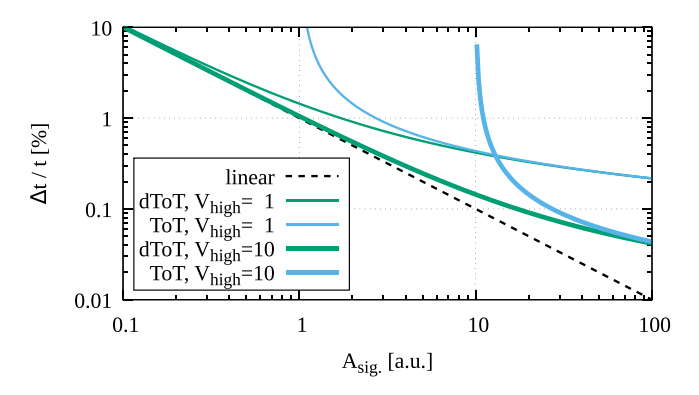


Fig. 3. Relative uncertainty of ToT and dToT measurements, shown for a value of $\sigma = 0.01$ in arbitrary units. The dToT curve interpolates between the linear signal shape and the logarithmic behavior of non-dynamic ToT, which cannot detect signals below V_{high} .

Fig. 3 illustrates how the uncertainty of the dToT implementation (5) interpolates between the linear (7) pulse and the non-dynamic ToT (6), achieving low uncertainty for small pulse amplitudes which remains low even at large amplitudes when $V_{\rm high}$ is chosen sufficiently large. For larger amplitudes, higher $V_{\rm high}$ values keep the relative uncertainty closer to that of a linear pulse.

4. Experimental results

The circuit was built with the component values in Fig. 1 and connected directly to the anode of photomultiplier coupled to a LaBr₂:Ce detector.² It was mounted face to face with a second identical detector, which was connected to a TwinPeaks front-end [3], and read out by a second TAMEX4 TDC. The MBS data acquisition system [4] was used to read out the TDC with the GOSIP protocol [5]. Three LYSO crystals (4 mm × 4 mm × 22 mm) were placed between the two LaBr₃:Ce detectors. The naturally radioactive 176 Lu in the LYSO crystals β -decays into 176 Hf which releases a cascade of three γ rays. These are used as additional lines for energy calibration and allow to measure the intrinsic time resolution of the setup. The resulting dToT histogram is shown in Fig. 4, with the green histogram indicating events coincident with the second LaBr3:Ce detector.

4.1. Energy calibration

The coincidence condition with the second detector allowed clear identification of peaks corresponding to ¹³⁸Ce at 789 keV and ¹³⁸Ba at 1436 keV. Both isotopes are decay products of the naturally radioactive 138La in the LaBr₃:Ce crystals. Dominant X-rays from both decay modes [6] provided a 32.9 keV calibration point. Three γ transitions from ¹⁷⁶Hf at 88.34 keV, 201.83 keV, and 306.78 keV [7] were also used in the calibration procedure.

Solving Eq. (3) for A_{sig} gives the calibration function:

$$A_{\text{sig}} = V_{\text{high}} \left(\exp \left(\frac{\text{dToT}}{\tau} \right) - k \right), \quad k = 1,$$
 (8)

which can be refined by allowing k to deviate slightly from 1 to account for non-ideal pulse shapes. The result of three-parameter fit is shown in Fig. 5.

4.2. Energy resolution

The low-energy section of the final spectrum is shown in Fig. 6. Energy resolution values (FWHM) were obtained via Gaussian fits to the visible peaks in the calibrated spectrum. Fig. 7 shows that the measured resolution matches the manufacturer specification of the detector resolution when interpolated to 661 keV. This result demonstrates that the simple dToT implementation allows to obtain energy spectra with the intrinsic energy resolution of LaBr3:Ce.

4.3. Time resolution

The timing performance of the dToT circuit was tested using coincident detection with the second detector. The radioactive decay of 176 Lu in LYSO crystals provides a $\gamma\gamma$ cascade that allows to measure the mean lifetime of the 4_1^+ state in ¹⁷⁶Hf. The $6_2^+ \rightarrow 4_1^+$ transition followed by the $4_1^+ \rightarrow 2_1^+$ transition can be selected by an energy gate in the $\gamma\gamma$ matrix (Fig. 8). The gated histogram of the leading-edge time difference between coincident pulses reflects the convolution of the time resolution of the detection system with the lifetime distribution of the measured 4⁺₁ lifetimes. The mean lifetime of that state was previously measured as $\tau_{4^{+}} = 130(8)$ ps [8].

The gated time-difference histogram is shown in Fig. 9. A Gaussianexponential convolution (9) was fitted to extract the mean lifetime as well as the time resolution of the setup.

$$f(\Delta t) = \frac{1}{2\tau} \operatorname{erfc}\left(\frac{\sigma}{\sqrt{2}\tau} - \frac{\Delta t}{\sqrt{2}\sigma}\right) \exp\left(\frac{\sigma^2}{2\tau^2} - \frac{\Delta t}{\tau}\right). \tag{9}$$

The resulting lifetime is $\tau_{4_1^+} = 127.7(13)$ ps, consistent with the previously measured value from [8]. Only statistical error of the fit result is given here. Discussion of systematic uncertainties of the mean lifetime value is beyond the scope of this work.

The time resolution of the combined TwinPeaks-dToT setup is $\sigma_{\text{TP,vs,dToT}} = 155(1)$ ps, corresponding to a FWHM resolution of 365(2) ps. A reference measurement with the same setup, but both detectors read out with the TwinPeaks front-end, yields $\tau_{4^+_1} = 131.1(12)$ ps and $\sigma_{\text{TP,vs,TP}} = 134(1)$ ps, corresponding to a FWHM resolution of FWHM 314(2) ps. From these results, the contribution of the dToT front-end can be estimated as:

$$\sigma_{\rm TP} \approx \frac{\sigma_{\rm TP, vs. TP}}{\sqrt{2}} \approx 95 \text{ ps},$$
 (10)

$$\sigma_{\text{TP}} \approx \frac{\sigma_{\text{TP.vs.TP}}}{\sqrt{2}} \approx 95 \text{ ps}, \tag{10}$$

$$\sigma_{\text{dToT}}(307 \text{ keV}) \approx \sqrt{\sigma_{\text{TP.vs.dToT}}^2 - \sigma_{\text{TP}}^2} \approx 125 \text{ ps}. \tag{11}$$

This is an approximation, because the two γ transitions are not at the same energy and the time resolution typically is better at higher amplitudes. Repeating the same procedure with gate A in Fig. 8 results in $\sigma_{\text{TP.vs.dToT}} = 169(1)$ ps and by applying Eq. $(11)\sigma_{\text{dToT}}(202\,\text{keV}) \approx$ 140 ps. Even though the results from TwinPeaks front-end with its specialized fast timing branch are not reached, the result shows that the developed dToT circuit does not drastically deteriorate the intrinsic timing performance of the LaBr3:Ce detector.

5. Conclusion

A simple dynamic time-over-threshold (dToT) circuit has been developed. The design uses direct feedback of the comparator output into the differential amplifier input, while using the detector capacitance for charge integration.

Analytical considerations show that the dToT implementation combines a broad dynamic range with excellent amplitude resolution. Experimental results confirm that the circuit preserves the intrinsic energy resolution of LaBr3:Ce, achieving FWHM values consistent with manufacturer specifications. Timing performance was also investigated in a $\gamma\gamma$ coincidence setup. The achieved leading-edge timing resolution is sufficient for fast nuclear lifetime measurements, albeit not fully matching the intrinsic detector resolution.

Future studies will investigate the count-rate capability and lowsignal performance of the circuit to further define its operating range.

 $^{^{2}\,}$ Model 25B25/2M-E1-LABR-X-NEG from SCIONIX HOLLAND BV.

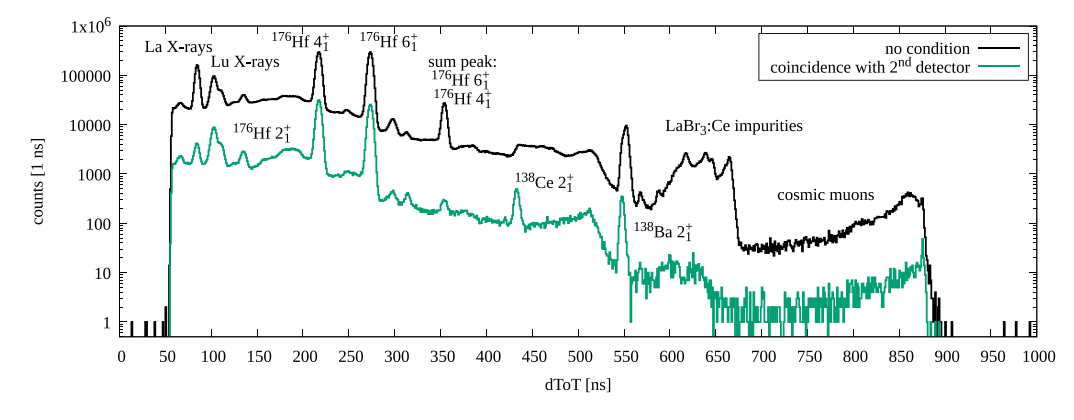


Fig. 4. Measured dToT histogram with the circuit in Fig. 1 and TAMEX4 TDC. Black: all hits; green: coincident with second detector.

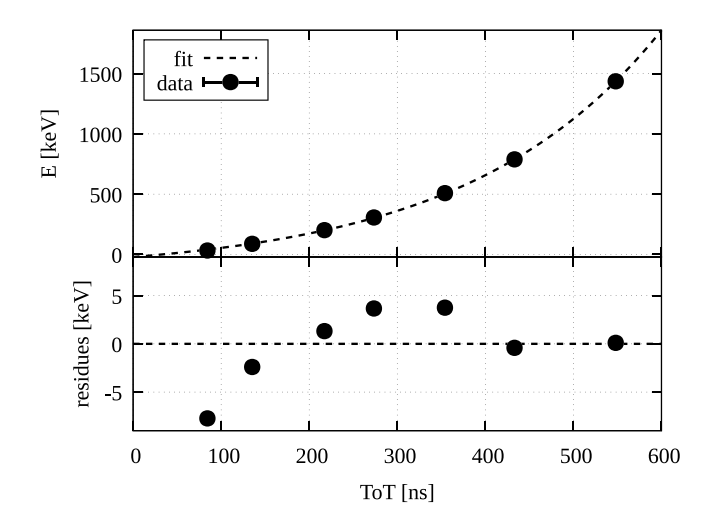
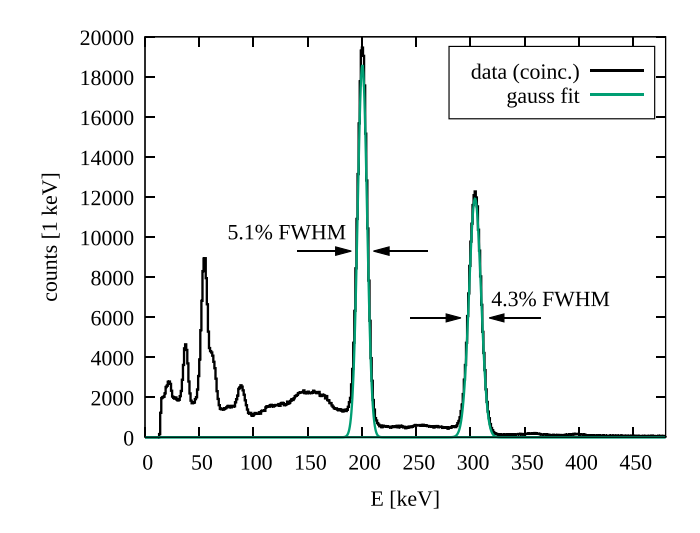
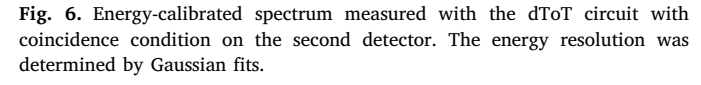


Fig. 5. dToT values of known gamma lines and fit using Eq. (8). Residuals (bottom) demonstrate good agreement. Error bars are smaller than symbol size.

Fig. 7. Energy resolution obtained with the dToT readout. Purple open point: manufacturer-specified 661 keV line.





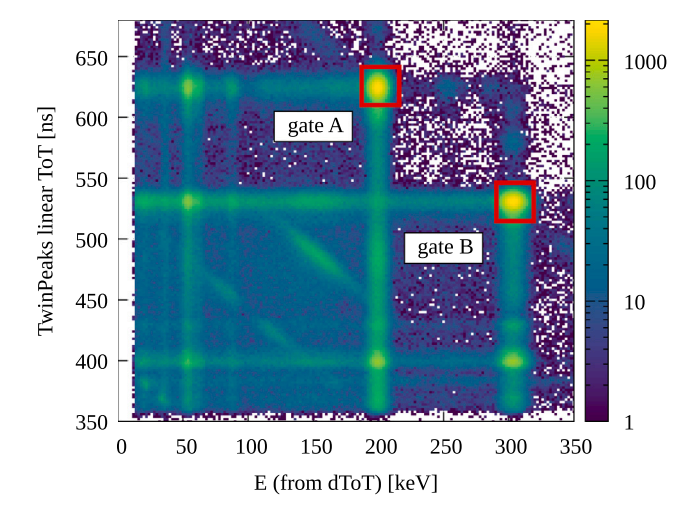


Fig. 8. Coincidence $\gamma\gamma$ histogram of dToT and TwinPeaks ToT. Red boxes: energy gates for time difference histograms. Gate B is used for Fig. 9.

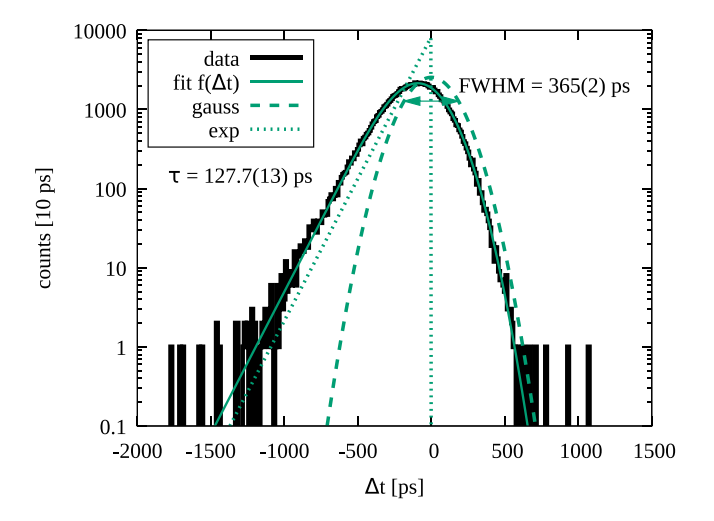


Fig. 9. Time distribution of leading-edge differences with an energy gate on the $6_2^+ \rightarrow 4_1^+ \rightarrow 2_1^+$ cascade, shown as gate B in Fig. 8. Green line: fit; dashed lines: components.

Declaration of generative AI and AI-assisted technologies in the manuscript preparation process

During the preparation of this work the author used ChatGPT in order to assist with grammar, spelling, and style corrections for improved readability. After using this tool, the author reviewed and edited the content as needed and takes full responsibility for the content of the published article.

Declaration of competing interest

The authors declare that they have no known competing financial interests or personal relationships that could have appeared to influence the work reported in this paper.

Acknowledgment

The publication is funded by the Open Access Publishing Fund of GSI Helmholtzzentrum für Schwerionenforschung, Germany.

Data availability

Data will be made available on request.

References

- [1] K. Shimazoe, H. Takahashi, B. Shi, T. Orita, T. Furumiya, J. Ooi, Y. Kumazawa, Dynamic time over threshold method, IEEE Trans. Nucl. Sci. 59 (6) (2012) 3213–3217, http://dx.doi.org/10.1109/TNS.2012.2215338.
- [2] Z. Song, Y. Wang, Y. Xiao, Q. Cao, Nuclear pulse charge measurement with a method of time over linear threshold, 2018, arXiv:1806.02494. https://arxiv.org/ abs/1806.02494.
- [3] A. Banerjee, M. Wiebusch, M. Polettini, A. Mistry, H. Heggen, H. Schaffner, H.M. Albers, N. Kurz, M. Górska, J. Gerl, Analog front-end for fpga-based readout electronics for scintillation detectors, Nucl. Instr. Meth. A 1028 (2022) 166357, http://dx.doi.org/10.1016/j.nima.2022.166357, https://www.sciencedirect.com/science/article/pii/S0168900222000389.
- [4] H. Essel, N. Kurz, The general purpose data acquisition system mbs, in: 11th IEEE NPSS Real Time Conference, 1999, pp. 475–478, http://dx.doi.org/10.1109/ RTCON.1999.842672.
- [5] S. Minami, J. Hoffmann, N. Kurz, W. Ott, Design and implementation of a data transfer protocol via optical fiber, in: 2010 17th IEEE-NPSS Real Time Conference, 2010, pp. 1–3, http://dx.doi.org/10.1109/RTC.2010.5750447.
- [6] J. Chen, Nuclear data sheets for a=138, Nucl. Data Sheets 146 (2017) 1–386, http://dx.doi.org/10.1016/j.nds.2017.11.001, https://www.sciencedirect.com/science/article/pii/S0090375217300753.
- [7] M. Basunia, Nuclear data sheets for a = 176, Nucl. Data Sheets 107 (4) (2006) 791–1026, http://dx.doi.org/10.1016/j.nds.2006.03.001, https://www.sciencedirect.com/science/article/pii/S0090375206000202.
- [8] J. Wiederhold, V. Werner, R. Kern, N. Pietralla, D. Bucurescu, R. Carroll, N. Cooper, T. Daniel, D. Filipescu, N. Florea, R.-B. Gerst, D. Ghita, L. Gurgi, J. Jolie, R.S. Ilieva, R. Lica, N. Marginean, R. Marginean, C. Mihai, I.O. Mitu, F. Naqvi, C. Nita, M. Rudigier, S. Stegemann, S. Pascu, P.H. Regan, Evolution of E2 strength in the rare-earth isotopes ^{174,176,178,180}Hf, Phys. Rev. C 99 (2019) 024316, http://dx.doi.org/10.1103/PhysRevC.99.024316, https://link.aps.org/doi/10.1103/PhysRevC.99.024316.